CHAPTER 4: VISCOELASTIC BEHAVIOR OF CARBON NANOTUBE-REINFORCED POLYMERS

Recent experimental results demonstrate that substantial improvements in the elastic properties of a polymer can be attained by using small volume fractions of carbon nanotubes as a reinforcing phase. While these preliminary results are intriguing, to date limited theoretical and experimental work has been done to investigate the impact of the nanotubes on the viscoelastic response of the polymer. Because the nanotubes are on the same length scale as the polymer chains, it is hypothesized that the polymer segments in the vicinity of the nanotubes will be characterized by a mobility that is different from that of the polymer chains in the bulk material. This reduced mobility, non-bulk polymer behavior, which we will refer to as an *interphase*, results in significant differences between the viscoelastic (VE) behavior of the bulk polymer and that of the nanotube-reinforced polymer. Experimental work presented in the literature, and our own experimental data described below, verify this phenomena (Shaffer and Windle 1999; Gong, Liu et al. 2000). As discussed in more detail in Chapter 2, such differences in VE response are typically characterized by:

1. increases in the low temperature (below the polymer glass transition temperature T_g) storage modulus,

2. significant increases in the high temperature (above T_g) stiffness of the material,

3. shifting of the effective glass transition temperature of the material, usually to temperatures greater than the T_g of the polymer, and

4. broadening of the loss moduli and loss tangent peaks.

In order to further characterize the viscoelastic response of nanotube-reinforced polymers, we have started an experimental program characterizing nanotube-reinforced polycarbonate. Samples for this study have been provided by Dr. Linda Schadler at Rensselaer Polytechnic Institute, who has extensive experience in the fabrication of nanotube-reinforced polymers (see (Schadler, Giannaris et al. 1998)). She has kindly provided well dispersed samples of 1 and 2 wt% MWNTs in polycarbonate (PC), as well as pure PC samples fabricated using an identical high temperature molding process. Samples with higher loadings of NTs are currently being developed and will be the subject of future studies (Schadler 2002).

Using dynamical mechanical analysis, three modes of viscoelastic response were tested for both pure and NT-reinforced polycarbonate:

1. temperature sweeps to measure the effective glass transition temperature of the samples,

2. frequency sweeps at different temperatures to determine the relaxation spectra of the samples, and

3. time domain creep/recovery tests to study the physical aging characteristics of the materials.

The results from each form of viscoelastic testing show that the viscoelastic behavior of the NRP is different than that of the pure polymer. This behavior is attributed to the nanoscale interactions between the embedded nanotubes and the polymer chains in the vicinity of the nanotubes, which in effect causes the composite to behave as the three phase (nanotube/interphase/matrix) composite shown in Figure 42.[1] If one assumes that the behavior of the nanotubes is purely elastic, then the differences in viscoelastic behavior between the pure polymer and the corresponding NRP must be due to changes in the viscoelastic response of this non-bulk polymer (interphase) region. It is worth noting that, in general, the viscoelastic behavior of polymer matrix composites with micron-sized inclusions closely mirrors that of the

---

[1] One could also argue that an appropriate model of the response would be that of a two-phase (nanotube-altered polymer) composite, where the nanotubes cause a uniform change in polymer properties throughout the composite. However, in the authors opinion such behavior is unlikely at the nanoscale. For low volume fractions of nanotubes, there are likely to be regions of polymer so removed from the embedded nanotubes that the polymer response in this region is unaffected by the nanotubes and hence identical to that of the bulk polymer.

pure polymer used as the matrix phase. Thus models of NRP viscoelastic behavior will have to be modified to account for this reduced mobility interphase region.

Our experimental results for each mode of viscoelastic behavior (T_g, relaxation spectra, and physical aging) are consistent with the hypothesis that this non-bulk polymer phase can be characterized by restricted molecular mobility. The effect of this restricted mobility region on each mode of viscoelastic response, as well as the advantages and disadvantages of each testing procedure, are given in Table 8.
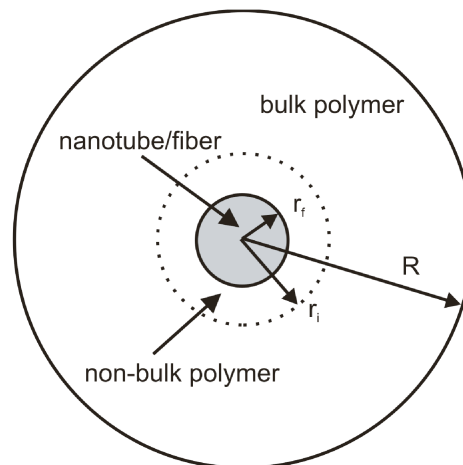
Figure 42. Three phase model of nanotube-reinforced polymer. Interphase thickness $t = r_i\text{-}r_f$.

	Glass transition temperature	Frequency response	Physical aging
Effective NRP behavior	Shift of T_g to higher temperatures	Broadening of the relaxation spectra to higher frequencies	Longer times needed to rejuvenate the sample; slower effective aging[2]
Strengths	Easiest to test	Micromechanics models available	Most sensitive to the addition of the NTs
Weaknesses	Shift in T_g is small; lack of T_g molecular models	More difficult than T_g analysis; less sensitive than physical aging	Most complicated to run; longer experimental times

Table 8. Modes of viscoelastic characterization.

In the sections that follow we will first present an introduction to viscoelasticity, focusing on a discussion of how the viscoelastic behavior of a polymer can be described based on the molecular mobility of the polymer chains. The influence of this molecular mobility on the glass transition temperature, time- and frequency-response of the material, and the physical aging characteristics of the polymer will follow. After briefly outlining the principles of dynamic mechanical analysis and the experimental tests that were conducted for this dissertation, we will present the experimental results of our testing of the glass transition temperature, frequency

---

[2] To date, complete rejuvenation to erase the thermal and mechanical history of the samples has yet to be achieved. However, our preliminary results lead us to believe that the long-term creep characteristics of the NRP sample will be significantly different from that of the bulk polymer. Further experimental work in this area is ongoing.

response, and physical aging of both blank (un-reinforced) and NRP samples. Included in the discussion of the frequency domain behavior will be initial modeling of the effective response using a frequency-domain Mori-Tanaka micromechanical approach. Such an approach may eventually lead to quantitative evaluation of the size and properties of the interphase region of the NRP via experimental results on macroscale-sized samples. We will conclude with a summary of the current results of this work and present future directions of research.

Introduction to Viscoelasticity

The classical theory of linear elasticity assumes that the stress and strain within a material are directly proportional in accordance with Hooke's Law, such that $\sigma = C\varepsilon$, where C is the stiffness tensor of the material and σ and ε are the stress and strain in the material, respectively. The response of an elastic material is independent of strain rate (and thus time and frequency) and temperature (other than thermal expansion effects). For an elastic material, removal of the applied stress (or strain) implies the material will return to its pre-deformed shape, such that the energy of deformation required to produce the deformation is recovered. Elasticity theory properly describes the mechanical behavior of a wide range of solids, particularly at low temperatures and low levels of strain. On the other hand, for a wide range of

fluids, the state of stress is proportional to the strain rate of the material but is independent of the strain, and is described for a Newtonian fluid as $\tau = \eta\dot{\varepsilon}$, where η is the viscosity of the fluid and τ and $\dot{\varepsilon}$ are the stress and the rate of strain of the fluid, respectively. The energy required to deform a Newtonian fluid cannot be recovered.

The Hookean Law for elastic solids and the Newtonian Law for viscous fluids are each idealizations of material behavior, however, and do not represent accurate mechanical models for a wide range of materials. In particular, these models are insufficient to describe the mechanical behavior of most polymer systems, whose behavior can be described as having both solid-like and liquid-like characteristics. Specifically, given an applied deformation some of the energy input into the system is stored within the material (elastic response), while some of the energy is dissipated as heat (viscous response). Materials that demonstrate such behavior are better described by viscoelastic models, which incorporate both elastic-like and viscous-like response characteristics. For such materials the mechanical response is time-dependent, and can be described in terms of an integral equation of the form

$$\sigma_{ij}(t) = \int_{-\infty}^{t} C_{ijkl}(t - \xi)\frac{d\varepsilon_{kl}(\xi)}{d\xi}\,d\xi \tag{59}$$

where σ_{ij} and ε_{kl} are the standard stress and strain tensors and C_{ijkl} is the time-dependent modulus. The viscoelastic behavior demonstrated by polymers is a direct

consequence of the complicated molecular motion that must underlie any mechanical deformation, as is described further in the next section.

Similar to the case of elasticity, given sufficiently small values of applied stress the response of the material is both superposable and scalable, such that when $\sigma = \sigma_1 + \sigma_2$, $\varepsilon = F(\sigma) = F(\sigma_1) + F(\sigma_2)$, and $\varepsilon = F(a\sigma) = aF(\sigma)$, where a is a constant. In such a case the response is described as linear, and we will limit our discussion in this dissertation to such conditions. A full discussion of viscoelasticity is beyond the scope of this dissertation; the reader is directed to several excellent textbooks have been devoted to this area (Ferry 1980; Aklonis and MacKnight 1983; Tschogel 1989).

Molecular theory of polymers and viscoelasticity

A polymer can be defined as a substance composed of molecules which have long sequences of one or more species of atoms or groups of atoms linked to each other by primary, usually covalent, bonds (Young and Lovell 1991). Thus on the nanoscale a polymer can be thought of as a "bowl of spaghetti", where the individual polymer chains are highly entangled, and in the case of thermosetting polymers, cross-linked at various points along the chain. Whereas deformation of a solid can be simply thought of as displacements of the atoms from an equilibrium position, polymer deformation requires highly cooperative motion amongst adjacent polymer chains (and perhaps between different segments of the same polymer chain). When subject to a

given load, instantaneous rearrangements of the polymer chains result in an initial configuration of the local polymer chains that represents the (momentary) minimum free energy of the system. However, if the state of deformation is maintained over time, long-range cooperative motion of the polymer chains will result in different minimal free energy configurations. While rearrangements on a local scale are relatively rapid, the long-range cooperative motion among the polymer chains can be quite slow; this results in the range of relaxation times which typically characterize viscoelastic behavior.

It is this continual rearrangement of the polymer chains that results in the viscoelastic behavior demonstrated by most polymers. The critical parameter describing how the polymer will respond to an applied strain (or stress) is the mobility of the polymer chains. The mobility of the polymer chains is influenced by both the chemical structure (the length of the chains, the size of the side groups which are attached to the backbone chain, and entanglements and/or cross-links among the chains, etc.) and the available thermal energy. Thus, polymers demonstrate both time-dependent (based on the range of time scales that describe various configurational rearrangements of the chains) and temperature-dependent properties. The vital parameter describing the temperature-dependent response of a viscoelastic material is the glass transition temperature T_g, which is described below.

Glass transition temperature

Every polymer system has a characteristic temperature, which is known as the glass transition temperature, below which thermal motions of the individual chains is greatly restricted (Ferry 1980). This glass transition temperature is typically thought of using the concept of *free volume*. Free volume is the unoccupied "empty space" on the nanoscale; it is the available space that the polymer chains can use to accommodate their rearrangements in configuration. At sufficiently high temperatures, enough free volume is present such that the chains can instantaneously achieve their equilibrium volume, and thus the material is in thermodynamic equilibrium. Polymers at such temperatures are soft (for thermoplastic polymers the material may be in the melt state); this is referred to as the rubbery region of the mechanical response.

However, as the temperature is reduced, the amount of free volume within the polymer decreases, until eventually the molecular motion of the chains is impeded due to a lack of free volume. Because of an insufficient amount of free volume (or alternatively, thermal energy), chain motion is restricted and the viscoelastic properties of the polymer are largely independent of time (or frequency). This is referred to the glassy or pseudo-elastic state of the polymer. The temperature marking

the critical free volume at which this transition occurs is called the glass transition
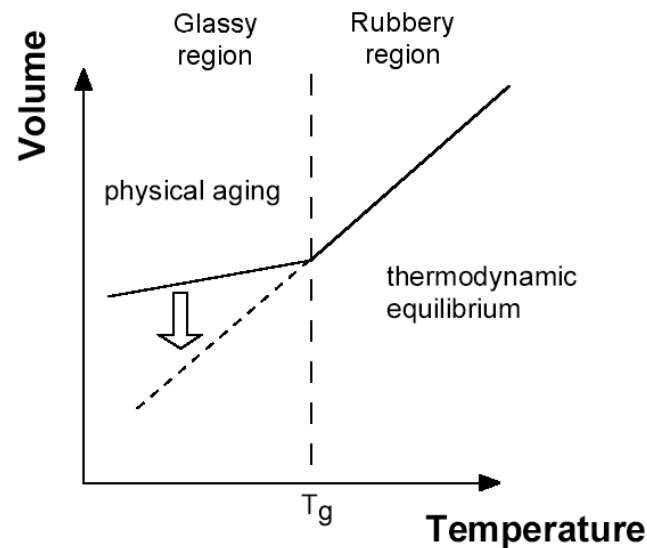
temperature, and is shown schematically in Figure 43.[3]

Figure 43. The glass transition temperature and physical aging.

Recall that a viscoelastic material is one that exhibits both elastic and viscous

behavior. From the standpoint of mechanical behavior, this implies that a portion of

the energy of deformation is recoverable (characterized by the storage modulus E')

and that a portion of the energy of deformation is irrecoverable (characterized by the

loss modulus E''). The ratio of the viscous to elastic components of the polymer

---

[3] While we will treat T_g as a discrete temperature, in reality slight deviations in the chain configurations at the nanoscale will result in a continuous transition from glassy to rubbery behavior.

response is designated the loss tangent *tan δ*, such that tan δ=E"/E'. The difference in mechanical behavior between the glassy and rubbery regimes is most evident when these material properties are measured as a function of temperature.

A common method of determining the glass transition temperature of a polymer is to use dynamic mechanical analysis (DMA). In this technique, the mechanical response of a polymer is probed as a function of temperature, and the temperature at which tan δ is maximum is assigned as the glass transition temperature. (Note that this definition of T_g is somewhat arbitrary, and while this definition is the most common, alternative definitions can be employed as discussed in the literature.) An example of the temperature dependence of the mechanical response for an epoxy sample is shown in Figure 44. The glass transition temperature for this sample is approximately 155 °C, and coincides with the sharp drop in storage modulus.

The glassy regime of behavior (for T < ~150 °C) is characterized by a stiff material response and a relatively constant storage modulus. As the test temperature approaches T_g, the storage modulus quickly decreases; this is referred to as the transition region of the mechanical response. For temperatures greater than T_g, the polymer response is described as rubbery, and displays a storage modulus that is orders of magnitude less than that of the glassy region. The behavior of the storage modulus in this region is strongly dependent on the chemical structure of the polymer. For thermoplastic polymers, the storage modulus will continually decrease as a

function of temperature as the polymer softens and ultimately melts at the melting temperature. For a thermoset system (such as the epoxy shown here), the rubbery region storage modulus will plateau at a relatively constant value until the polymer begins to degrade at sufficiently high temperatures.
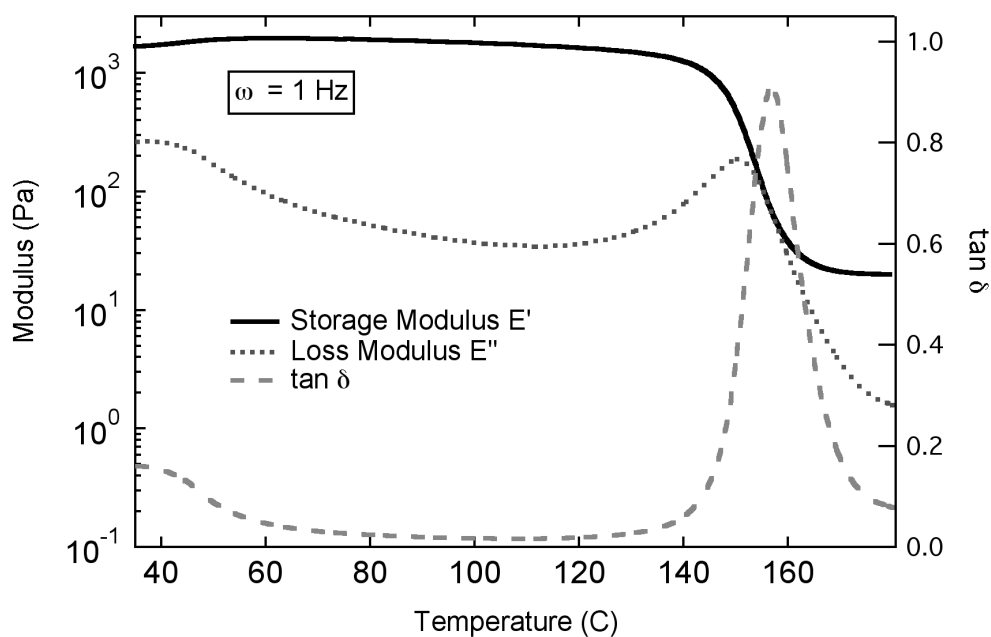
Figure 44. Temperature dependence of the modulus of an epoxy sample.

More information regarding the technique of dynamic mechanical analysis, along with definitions of the various viscoelastic moduli, is provided later in this Chapter. Other experimental techniques can also be used measure the T_g of polymer samples, including differential scanning calorimetry (DSC) and thermomechanical

analysis (TMA); however, DMA is very sensitive to the changes in the underlying structure of the material and is particularly suited for transition measurements (Menard 1999).

Physical aging

Referring to Figure 43, below the glass transition temperature the material is not in thermodynamic equilibrium, as sufficient free volume is not available for the polymer chains to instantaneously achieve the minimal free energy state. Thus as the sample remains below T_g, long-scale cooperative coordination of the polymer chains will gradually allow the polymer to reach its thermodynamic equilibrium state. As this gradual evolution towards thermodynamic equilibrium takes place, material properties such as specific volume and modulus will also continuously change (Struik 1978). This process is known as *physical aging*, and is dependent on the thermal history of the sample. Because the mechanical properties of the polymer change as a result of physical aging, physical aging can have a large impact on the long-term properties of polymeric materials. For a more in-depth discussion of physical aging, the reader is referred to the literature (Struik 1978; Ferry 1980).

Physical aging is a thermoreversible process, and as such is distinct from degradative processes such as chemical aging and damage. If the sample is heated for a sufficient time above the glass transition temperature, the thermal history of the

sample is erased; this is a process called *rejuvenation*.[4] Once a sample has been rejuvenated, it loses all "memory" of it past thermal history. Upon a subsequent quench to below T_g, the process of physical aging then starts anew. The time spent below T_g, relative to the last rejuvenation, is called the aging time t_e.
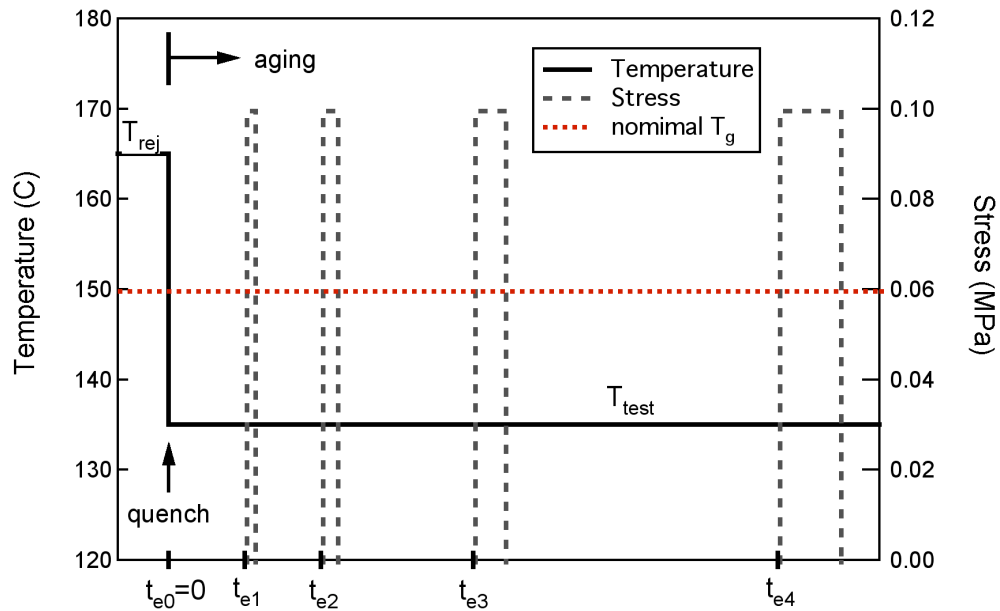

Figure 45. Isothermal physical aging test method of Struik.

Characterization of the isothermal physical aging characteristics of a polymer are typically carried out using the short-term creep test method developed by Struik

---

[4] While rejuvenation is typically thought of an instantaneous process occurring once the material is above T_g, in reality thermal gradients within the sample and other factors make it necessary to maintain the sample above T_g for a sufficient period of time before total rejuvenation takes place.

(1978) and described schematically in Figure 45.[5] After the material has been rejuvenated above T_g for a sufficient period of time, the sample is quenched to the test temperature T_{test} and maintained at this temperature for the duration of the test.

At different aging times t_e (time since quench), the sample undergoes a short-term creep test. The duration of the short-term test is 10% of the aging time at the start of the test, to ensure that further aging of the sample during the shot-term creep test is negligible. At the end of each loading step, the applied load is removed and the sample allowed to recover until the start of the next short-term creep test. Typically the aging times at the start of each short-term test are chosen such that $t_e^{i+1} = 2t_e^i$. (For the experimental work discussed later in this chapter, the initial aging time was 45 minutes.) From each short-term creep test, a momentary compliance curve is obtained as shown in Figure 46 for a pure polycarbonate sample. As expected, during each individual creep test the compliance *S(t) decreases* (i.e. the stiffness *increases*) due to the molecular rearrangements of the polymer chains, which suggests a loss of chain mobility due to physical aging.

For typical physical aging of polymeric materials, the compliance curves at different aging times can be superposed through a horizontal shift. Analogous to the more standard shifting of material responses in time and frequency space (time-

---

[5] This method has also been extended to study the nonisothermal physical aging of polymeric materials (Bradshaw 1997).

temperature superposition, which is discussed in the next section), this shifting of momentary compliance curves is referred to as *time-aging time superposition*. Typically the momentary compliances at different aging times are shifted to the largest aging time, as this represents the compliance curve for which the greatest number of data points has been collected. An example of the shifting of the momentary compliance curves to create a reference momentary compliance curve, based on the polycarbonate data shown in Figure 46, is shown in Figure 47. The amount of shifting necessary to superpose the momentary compliance curve at aging time t_e to the reference aging time $t_{e,ref}$ is referred to as the aging time shift factor a_{t_e}.
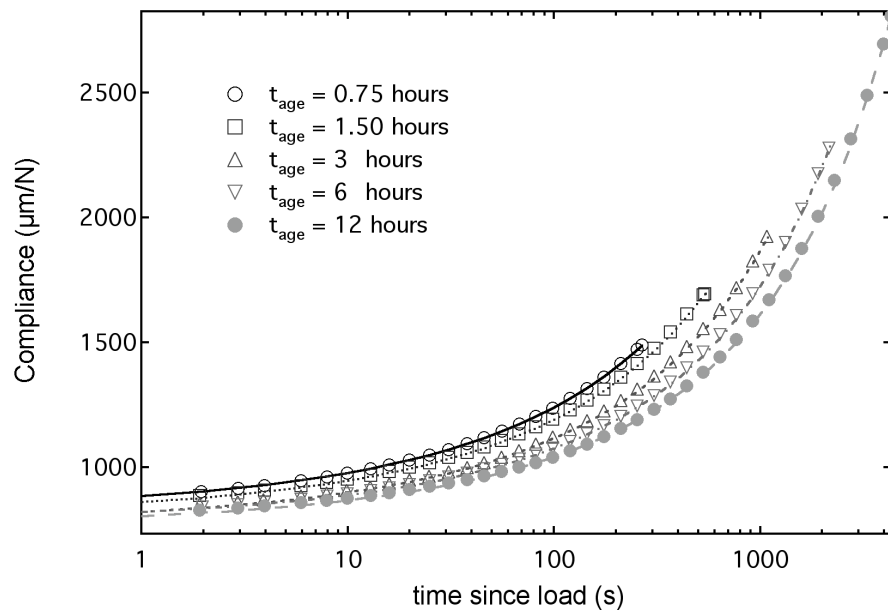
Figure 46. Short-term momentary compliance curves for different aging times (pure PC sample, rejuvenated at 165 °C for nominal 15 minutes).
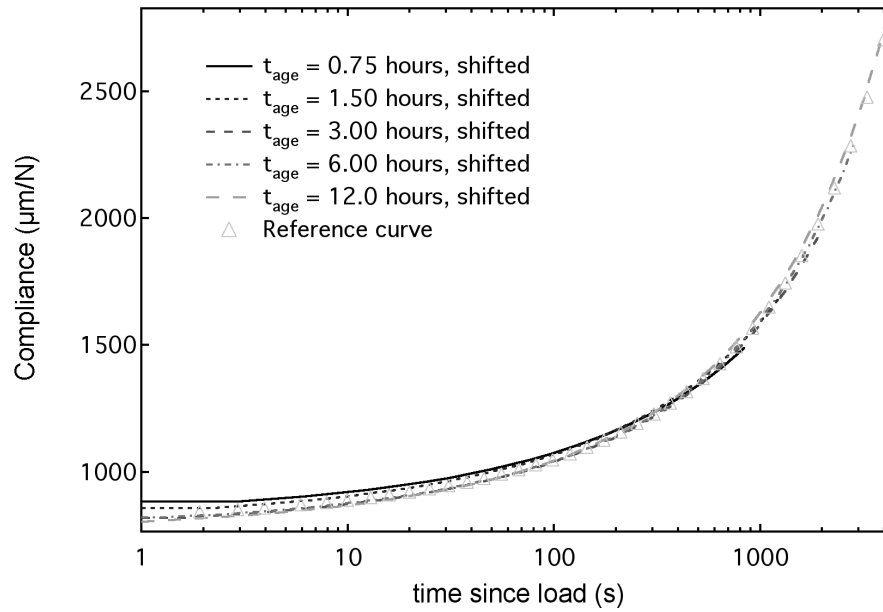
Figure 47. Shifting of momentary compliance curves to form a reference curve (pure PC sample, rejuvenated at 165 °C for nominal 15 minutes).

For a specimen isothermally aged at a given temperature $T<T_g$, it has been shown experimentally that the aging time shift factors a_{t_e} are linearly related to the aging time in log-log space via the *shift rate* μ, such that

$$\mu = -\frac{d\log a_{t_e}}{d\log t_e}.$$ (60)

This relationship is shown in Figure 48 for the same polycarbonate data presented earlier. The shift rate μ is a material parameter that may be used to determine the momentary compliance (and hence the modulus) at a particular aging time given an

aging time reference curve. For most polymer materials, the shift rate μ is on the order of 1 (Brinson and Gates 1995).[6]

Data reduction for all physical aging experimental data (including that presented above) was carried out using PHYAGE, a program developed at Northwestern to characterize the isothermal physical aging of polymers. The program uses an error minimization routine to fit an appropriate function to the experimental compliance data, and then proceeds to find the optimal reference curves and shift rates describing the physical aging of the polymer. Details of the program are provided elsewhere (Bradshaw and Brinson 1997c; Bradshaw and Brinson 1997a).

The fact that the momentary compliance curves at different aging times can be superposed via a horizontal shifting procedure demonstrates that on the nanoscale physical aging has the effect of altering the relaxation times (and thus the molecular mobility) characteristic of the polymer. Thus we suspect that the embedded carbon nanotubes may alter the physical aging response of the polymer, when compared to physical aging of the un-reinforced sample. Later in this chapter we will present our initial findings in this regard, which seem to verify this hypothesis.

---

[6] Given a sufficiently long period of physical aging, the material will eventually reach effective equilibrium, which is characterized by an order of magnitude decrease in the shift rate (McKenna, Leterrier et al. 1995). However, effective equilibrium is not considered in the present work.
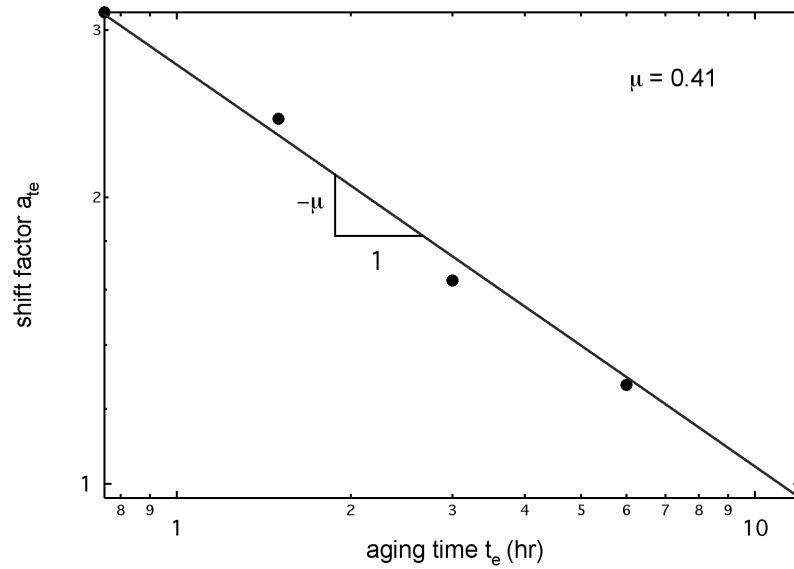
Figure 48. Shift factors and the shift rate μ describing physical aging. (Data for pure PC sample, rejuvenated at 165 °C for nominal 15 minutes)

Time- and frequency- domain response

Based on the previous discussion of the molecular structure of polymers, it is not surprising that such materials exhibit time-dependent properties. The viscoelastic time-dependent modulus can be characterized by a Prony series representation of the form

$$E(t) = E_\infty + \sum_{j=1}^{N} E_j e^{-\frac{t}{\tau_j}}, \tag{61}$$

where E_∞ is the rubbery asymptotic modulus, E_j are the Prony series coefficients,

and τ_j are the relaxation times. Taking the half-sided Fourier transform of (61) yields[7]

$$\overline{E}(\omega) = \int\limits_0^\infty E(t)e^{-i\omega t}\ dt, \tag{62}$$

where i is the imaginary number. The frequency-domain response is described by the

complex modulus $\overline{E}^*(\omega)$, which is defined as

$$, \tag{63}$$

$$E'(\omega) = E_\infty + \sum_{j=1}^N \frac{E_j\omega^2}{\dfrac{1}{\tau_j^2} + \omega^2} \tag{64}$$

$$E''(\omega) = \sum_{j=1}^N \frac{\dfrac{E_j}{\tau_j}\omega}{\dfrac{1}{\tau_j^2} + \omega^2} .$$

The terms defined in (64) are referred to as the storage modulus $E'(\omega)$ and loss

modulus $E''(\omega)$, respectively.[8] The storage modulus is a measure of the energy stored

---

[7] While this is generally referred to as a Fourier transform, note that it is missing the factor of $1/2\pi$ that typically appears in the standard definition of the Fourier transform.
[8] Such notation follows the standard convention of viscoelasticity, where the use of single primes and double primes denote storage (elastic) and loss (viscous) components of a complex material function, respectively. This notation will be used throughout this dissertation.

and recovered by a viscoelastic material per cycle of sinusoidal deformation, whereas the loss modulus is a measure of the energy dissipated as heat during a similar cycle (Tschogel 1989). Note that as written in (64) both the storage and loss moduli are real quantities.

The ratio of the loss modulus to the storage modulus is referred to as the loss tangent *tan* δ, such that

$$\tan\delta = \frac{E''}{E'}.$$ (65)

The loss tangent is related to the ratio of energy loss to energy stored in the deformation cycle. Note that the loss tangent is a dimensionless parameter. An example of the storage and loss moduli and the tan δ as a function of temperature (for a constant frequency, sinusoidal deformation) was given previously in Figure 44.

Time-temperature superposition

While experimental measurements of the polymer response can in theory be measured for any length of time, time scales on the order of months or years would be impractical for most applications. Here one can use the principle of time-temperature superposition, a method of reduced variables, in order to extend the time scales (by many orders of magnitude) of the response at a particular temperature of interest. For example, since experimental data may only be available over a limited range of

frequencies, the principle of time-temperature superposition is extremely useful in that it can extend the range of frequencies over which the material behavior can be studied. Because time-temperature superposition is a standard tool for the analysis of experimental viscoelastic data, it will only be briefly described below. The reader is referred to any classical book on viscoelasticity for a more precise treatment; see for example Ferry (1980).

The basic principle of time-temperature superposition (analogous to time-aging time superposition described previously) is that the material behavior at different temperatures can be superposed via horizontal shifting in log-log space to form a reference (or master) curve at a given temperature. This permits one to have a measure of the polymer response over a range of time (or frequency) scales using data collected within experimental accessible time scales.

This procedure is demonstrated using creep compliance data collected on an epoxy sample as shown in Figure 49 (O'Brien, Mather et al. 2001). Here data is collected over a relatively short time range (up to approximately 100 s) at temperatures ranging from 30 °C to 175 °C. These individual creep compliance curves are then shifted to the right (higher temperatures are shifted further and correspond to longer times) and superpose to form the master reference curve at 30 °C. Thus using time-temperature superposition, the material behavior at 30 °C is now available over approximately 14 orders of magnitude, which would certainly be inaccessible

experimentally. Mathematically, the shifting of material response data collected at different temperatures can be expressed as

$$E(t;T_1) = E(\frac{t}{a_T};T_{ref}),$$ (66)

where a_T is referred to as the temperature shift factor and T_{ref} is the temperature of the master curve.

Frequency-domain data collected at different temperatures can be shifted in an equivalent manner, providing the material response at a given temperature over a large range of frequencies. Occasionally slight vertical curve shifting will be required (this is true for both the time and frequency domain experimental data); often the basis of this vertical shifting is the temperature-dependence of the polymer density as discussed further in the literature (Ferry 1980; Aklonis and MacKnight 1983). Because time-temperature superposition was only used here as a means to extend the range of frequencies available for the collection of experimental data, further discussion of topics associated with time-temperature superposition (such as the standard WLF representation of the temperature shift factors) is not warranted here. The reader is referred to the literature for further reading in this area (Ferry 1980; Aklonis and MacKnight 1983).
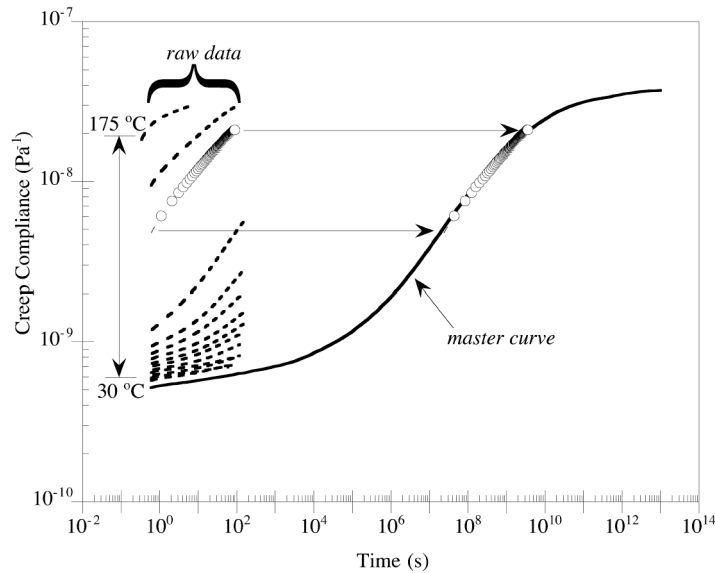
Figure 49. Time-temperature superposition for the creep compliance of an epoxy. T_{ref}=30 °C. (O'Brien, Mather et al. 2001).

Relaxation spectrum

As the number of the Prony series elements representing the time dependent modulus in (61) goes to infinity, one obtains a continuous spectrum of relaxation times describing the viscoelastic response of the polymer. In this case, the time-dependent modulus can be expressed as

$$E(t) = E_\infty + \int_{-\infty}^{\infty} H(t) e^{-\frac{t}{\tau}} d(\ln \tau) \qquad (67)$$

where H(t) is referred to as the relaxation spectrum. The relaxation spectrum represents the infinitesimal contributions to the modulus from relaxation times lying in the range from τ to $\tau + d\tau$. The relaxation spectrum is useful in qualitatively gauging the distribution of relaxation mechanisms (and hence, again, molecular mobility) at different time scales (Ferry 1980). Thus the relaxation spectrum will give us a qualitative manner in which to analyze the impact of the embedded nanotubes on the relaxation mechanisms of the nanotube-reinforced polymer.

For our purposes it will suffice to use Alfrey's approximation of the relaxation spectrum, which is defined as

$$H(t) \approx -\frac{dE(t)}{d\ln(t)}. \tag{68}$$

Thus the relaxation spectrum can be approximated as the negative slope of the time-dependent modulus (Ferry 1980). Assuming that a Prony series representation of the time-dependent modulus is known, the relaxation spectrum can thus be approximated via the analytical expression

$$H(t) \approx \sum_{j=1}^{N} \frac{t}{\tau_j} E_j e^{-\frac{t}{\tau_j}}. \tag{69}$$

Equation (69) was used to approximate the relaxation spectra for the different samples, and used the Prony series elements determined from the curve-fitting procedure described later in this Chapter.

An interphase region in nanotube-reinforced polymers

Because the nanotubes are on the same length scale as the polymer chains, it is anticipated that the NTs will alter the local polymer morphology in the region directly surrounding the nanotube (see Figure 42). We refer to this region of non-bulk polymer behavior as the interphase, borrowing a term used in the composites community that refers to the region separating the fiber and matrix phases. Due to changes in the local chain structure of the polymer, the interphase region will have mechanical properties different from those of the bulk polymer. While in traditional composites research the interface region is generally attributed to a host of factors (such as the use of fiber sizings, mechanical imperfections, unreacted polymer components, etc.), here we limit our discussion specifically to the change in molecular mobility of the polymer chains in this region due to the presence of, and interactions with, the nanotube inclusions.

Recent experimental work has estimated the interphase thickness for carbon fiber-epoxy composites to be on the order of 1 μm for a 25 μm diameter fiber (Thomason 1995; Mai, Mader et al. 1998). Because the interphase region makes up a very small fraction of the micron-sized fiber composite, its impact on the overall

viscoelastic response of the material is often neglected. However, recent molecular dynamic simulations of NRPs suggest that the local changes in the polymer structure are on the same length scale as the diameter of the NT, as shown in Figure 50 for a SWNT/PmPV/LaRC-SI composite system. (Odegard, Gates et al. 2001b; Wise and Hinkley 2001). In this case, the volume fraction of the interphase within an NRP will be much larger than the interphase region in a micron-sized composite.

For the system shown in Figure 50, poly(m-phenylenevinylene) (PmPV) is used to enhance the interfacial characteristics of the system, as it has been shown that such molecules tend to helically wrap themselves around the nanotube (Lordi and Yao 2000). From Figure 50 we see that the local density of the polymer molecules is greater in the vicinity of the nanotube, which from a molecular standpoint can be viewed as reducing the molecular mobility of these polymer chains (in comparison to those exhibiting bulk polymer behavior). It is hypothesized that such behavior will also be exhibited in nanotube-reinforced polymer systems without the use of an interfacial polymer, although much more work in this area is required.
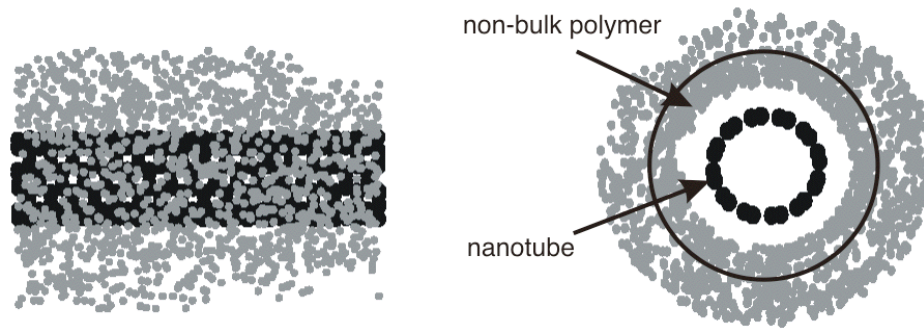
Figure 50. Equilibrium structure of a (6,6) SWNT/PmPV/LaRC-SI composite system based on molecular dynamics simulations (Odegard, Gates et al. 2001b).

Because the nanotubes have significantly more surface area (per unit volume) than micron-sized inclusions, a significant fraction of the polymer in NRP systems will be in the near vicinity of an embedded nanotube, and thus may be characterized by this non-bulk behavior. From simple geometric considerations (see Figure 42), the volume fraction of the interphase region V_i is related to the volume fraction of the fiber/nanotube inclusion V_f and the thickness of the interphase region t as (Fisher and Brinson 2002)

$$V_i = \left[2\left(\frac{t}{r_f}\right) + \left(\frac{t}{r_f}\right)^2 \right] V_f = \beta V_f. \tag{70}$$

Likewise, the ratio of the volume fraction of the non-bulk polymer phase (interphase) to the total volume fraction of viscoelastic phases within the composite (interphase and matrix) can be expressed as

$$\frac{V_i}{V_i + V_m} = \frac{\beta V_f}{1 - V_f}.$$

(71)

These expressions are shown graphically in Figure 51 as a function of fiber/nanotube volume fraction for various ratios of interphase thickness t to fiber radius r_f. Representative values of (t/r_f) are on the order of 0.05 for carbon fiber composites (Thomason 1995) and 1.0 for nanotube-reinforced polymers (Wise and Hinkley 2001), respectively.

From Figure 51, we see that for the case of nanotube-reinforced polymers (where the ratio t/r_f is on the order of 1.0), a significant portion of the NRP can be characterized as the interphase region. In this case, the non-bulk polymer behavior of the interphase region is expected to contribute to the overall viscoelastic response of the material. For the case for traditional micron-sized fiber polymer composites, where the ratio t/r_f may be on the order of 0.05, the interphase region is much smaller and often neglected in micromechanical predictions of effective properties.[9] We note that Figure 51 suggests that the interphase volume fraction will be appreciable for even relatively low loadings of nanotube inclusions.

---

[9] Fiber sizings are known to significantly enhance the fiber-matrix interface in traditional polymer matrix composites. However, because the interphase region in such systems is typically small, it is often neglected in micromechanical predictions for the effective modulus of these materials.
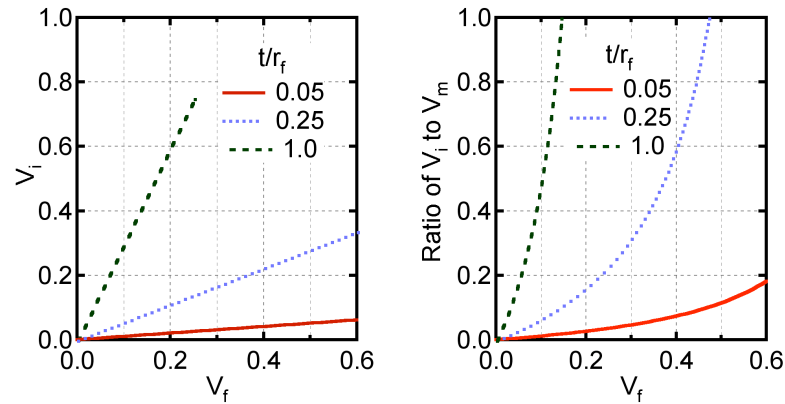
Figure 51. Interphase volume fraction (V_i) (left) and ratio of the interphase (non-bulk) to matrix (bulk) volume fraction (V_m) (right) as a function of fiber volume fraction V_f.

Perhaps the simplest means to model this non-bulk polymer behavior is to assume a distinct interphase region, within which interactions between the nanotubes and the polymer chains alter the characteristic relaxation times of the material. Recalling the Prony series form for a viscoelastic modulus discussed previously, the change in relaxation times of the interphase region can be modeled via the introduction of a mobility parameter α, which relates the mobility (and hence the mechanical properties) of the interphase to that of the pure polymer matrix (Fisher and Brinson 2002), such that[10]

---

[10] It is also likely that interactions between the polymer chains and the nanotubes will result in changes in the magnitude of the time (and frequency) domain moduli of the interphase region with respect to that of the pure polymer. Such changes could be incorporated into this model via multiplication of the Prony coefficients E_j. Such modeling efforts will be pursued in future work.

$$E(t) = E_\infty + \sum_{j=1}^{N} E_j \, e^{-\frac{t}{\alpha \tau_j}}.$$
(72)

The effect of the mobility parameter α on the time domain modulus of the material is shown schematically in Figure 52. In this manner the mobility parameter α can be used to qualitatively characterize the change in mechanical properties of the non-bulk polymer phase. For $\alpha < 1$ the polymer chains are more mobile, which shifts the transition region of the time-dependent response to shorter times. For $\alpha > 1$, the opposite is true and the response of the non-bulk phase is stiffer than its bulk polymer counterpart. By definition, $\alpha = 1$ describes the bulk polymer response. Assuming such a form for the mechanical properties of the non-bulk polymer interphase region, one can use various micromechanical models to interpret experimental data for carbon nanotube-reinforced polymers. Such a procedure will be demonstrated later in this chapter.
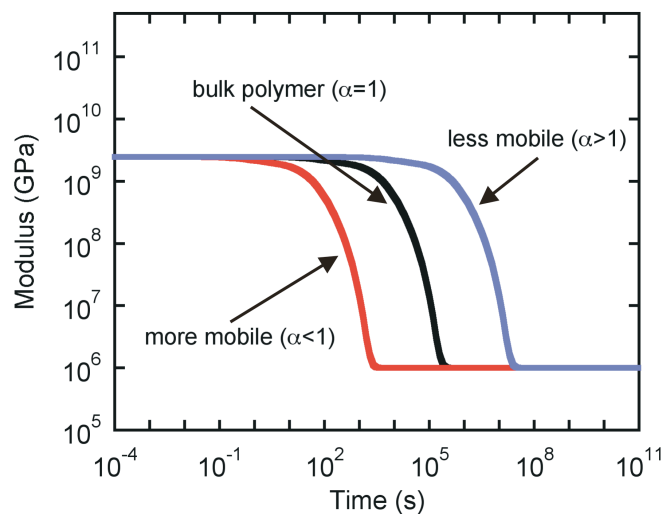
Figure 52. Time-dependent modulus as a function of the mobility parameter α.

Experimental Procedures

All experimental data described in this dissertation were collected using a TA Instruments DMA 2980 dynamic mechanical analyzer with a special film tension clamp (see Figure 53). Critical instrument specifications are as follows: temperature range from −150 to 600 °C (using liquid nitrogen as a coolant), frequency range from 0.001 to 200 Hz, and a maximum applied force of 18 N. The film tension clamp was designed for specimens between 5 to 30 mm in length, up to 8 mm in width, and up to 2 mm in thickness. Typical lengths of the polycarbonate samples tested were (length *x* width *x* thickness) 10 *x* 6 *x* 0.5 mm.
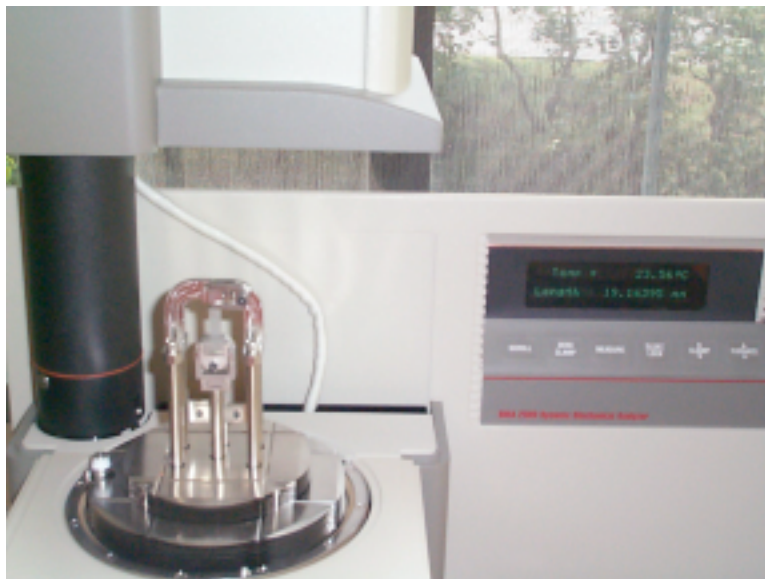
Figure 53. TA Instruments DMA 2980 with film tension clamp.

Nanotube-reinforced polycarbonate samples were provided by Dr. Linda Schadler at RPI, who has extensive experience fabricating nano-reinforced polymer samples. The samples were fabricated using a high-temperature molding operation that is proprietary. Currently we have received and tested both pure polycarbonate samples (fabricated using the same method as used for the reinforced polymer samples) and samples with 1 and 2 wt% embedded MWNTs; additional samples with other weight fractions of MWNTs will be tested in the future. The MWNTs used in the samples were provided by Dr. Rodney Andrews at the University of Kentucky, and were grown via chemical vapor deposition using Xylene-ferrocene as the carbon source. The outer diameters of the nanotubes are on the order of ~25 nm. These samples are believed to have an excellent dispersion of nanotubes (Schadler 2002), and based on

Dr. Schadler's expertise in this area (Schadler, Giannaris et al. 1998; Ajayan, Schadler et al. 2000; Siegel, Chang et al. 2001), we believe these samples represent high-quality nanotube-reinforced polymers.

The samples were received from Dr. Schadler in the as-molded shape and stored for at least 24 hours in a room temperature desiccator using Drierite (Xenia, OH) as a desiccant. For DMA analysis, the samples were cut to size using a Struers (Cleveland, OH) Accutom-5 saw with a diamond blade (300 CA) running at 1000 rpm and a feed speed of .05 mm/s, using water as a coolant. The cut edges were then polished using 240 and 600 grit Carbimet grinding paper from Buehler (Lake Bluff, IL). Then samples were then returned to the desiccator for a period of at least 24 hours, and maintained in the desiccator until removed for testing.

Three types of viscoelastic testing were conducted using the DMA 2980. For temperature sweeps to measure the glass transition temperature, the samples were subjected to a sinusoidal displacement of 3 μm (resulting in strains less than 0.1%) at a constant frequency of 1 Hz. After inserting the sample into the DMA, but prior to load, the sample was held isothermally at the initial test temperature (typically just above room temperature) for 10 minutes so that thermal equilibrium was established. The sinusoidal deformation was then initiated, and the temperature was ramped at 2°C/min until the final test temperature was reached (typically T_g + 30°C for the pure polycarbonate samples and T_g + 50°C for the reinforced samples).

For the testing of the frequency-domain response of the samples, the samples were held isothermally at the initial test temperature (typically 100 °C) for 15 minutes. The samples were then subjected to sinusoidal deformation at a constant amplitude of 3 μm, at discrete frequencies from 200 to 0.2 Hz (five frequencies per decade, evenly spaced in log frequency space). After the testing at a particular temperature was completed, the temperature was raised 5°C (taking less than 1 minute), held isothermally for 5 minutes, and then the frequency scanning at the new test temperature conducted. This procedure was repeated until the measurements at the final test temperature (170 °C for the pure PC, 200 °C for the reinforced-samples) had been obtained.[11]

For the physical aging tests, the DMA 2890 was used in creep mode with an applied stress of 0.1 MPa (during the load portions of the testing). The sample was first equilibrated at the test temperature (below T_g, T_{test}=135 °C for all results presented in this dissertation) for a nominal time of 10 minutes.[12] The chamber temperature was then increased to the rejuvenation temperature T_{rej} and held for a nominal length of time t_{rej}. (The two rejuvenation procedures described later in this

---

[11] A stark difference between the behavior of the pure and reinforced PC samples was evident in this testing procedure. Whereas tests with the pure PC were prematurely ended ~175°C due to severe elongation of the sample caused by flow, an identical testing methodology conducted on the reinforced PC samples was able to go to 200 °C with no apparent degradation in sample geometry.

[12] All times describing the procedure for the physical aging tests are nominal times in that they are measured from the beginning of the temperature jump, and not once the desired temperature has been reached.

chapter are 160 °C for 10 minutes and 165 °C for 15 minutes; note that t_{rej} is always greater than the *actual* time the sample was at the rejuvenation temperature due to thermal lag effects.) Once the rejuvenation step has been completed, the sample is quenched to T_{test} by jumping the setpoint of the heater controller to the test temperature, which in effect shuts off power to the heater until T_{test} was reached via ambient cooling.[13] At the start of the quench step the aging time is set to zero; load/unload tests were then conducted at an initial aging time of 22.5 minutes and then repeated at 3/4, 1.5, 3, 6, and 12 hours as outlined in Figure 45. Because it took approximately five minutes for the DMA chamber to establish equilibrium at T_{test}, the data collected at 22.5 minutes was not included in our analysis below (due to nonisothermal aging effects). A preload of 0.01N was maintained on the sample throughout both the load and unload portions of the test.

---

[13] Initial tests were also conducted using a liquid nitrogen cooling accessory, purchased from the DMA manufacturer, during the quench phase of the test. However, because the time to quench was only slightly faster using the liquid nitrogen accessory (approximately 3 minutes using the liquid nitrogen accessory versus 5 minutes by effectively shutting off power to the heater), the liquid nitrogen accessory was not used during the quench steps.

Glass Transition Temperature for Nanotube-reinforced Polycarbonate

Perhaps the most straightforward manner to evaluate changes in viscoelastic behavior is to measure the glass transition temperature of a sample using the constant frequency-constant amplitude temperature scan method outlined earlier in this chapter. Using this procedure, the storage and loss moduli and the loss tangent of the material are measured as a function of temperature; the results of such scans on the blank and NT-reinforced polycarbonate systems are shown in Figure 54-Figure 56, respectively.
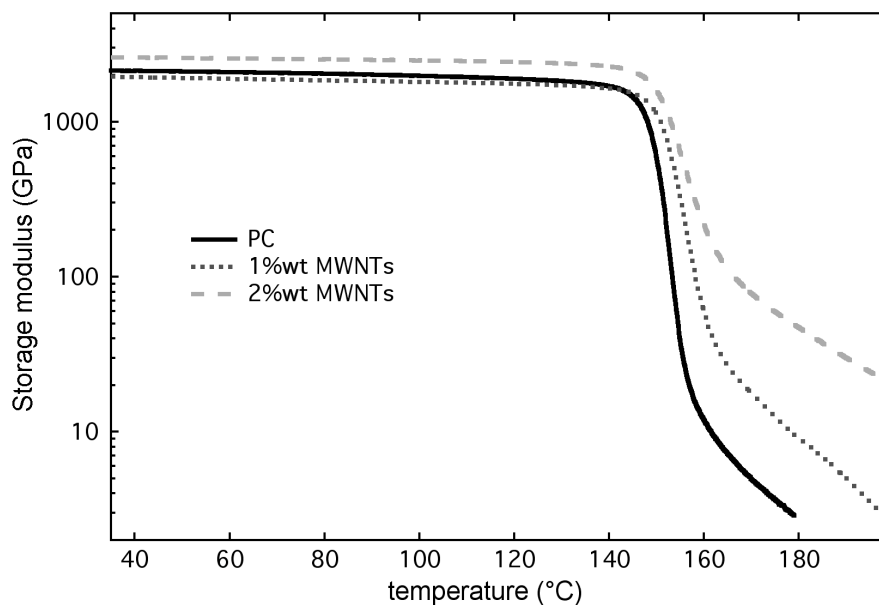
Figure 54. Storage moduli as a function of temperature for PC samples.
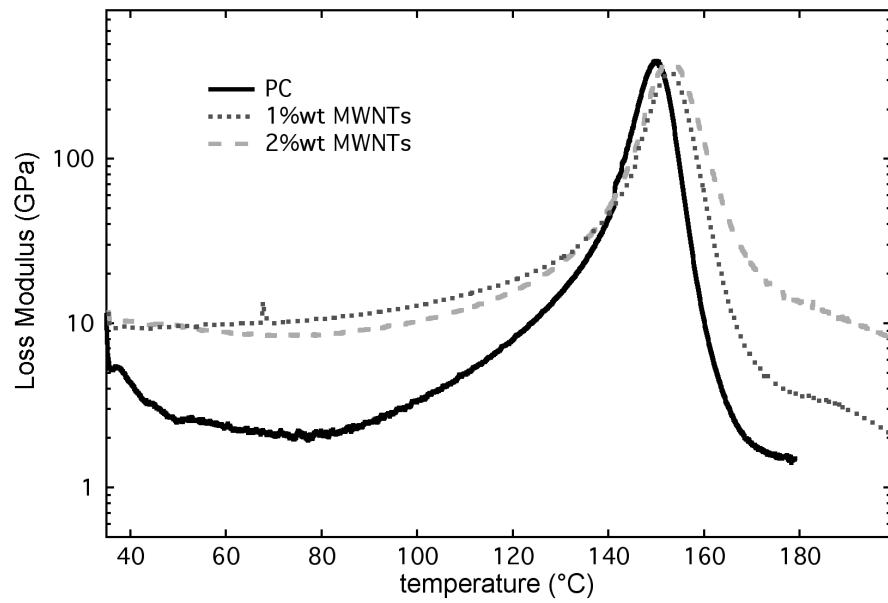
Figure 55. Loss moduli as a function of temperature for PC samples.
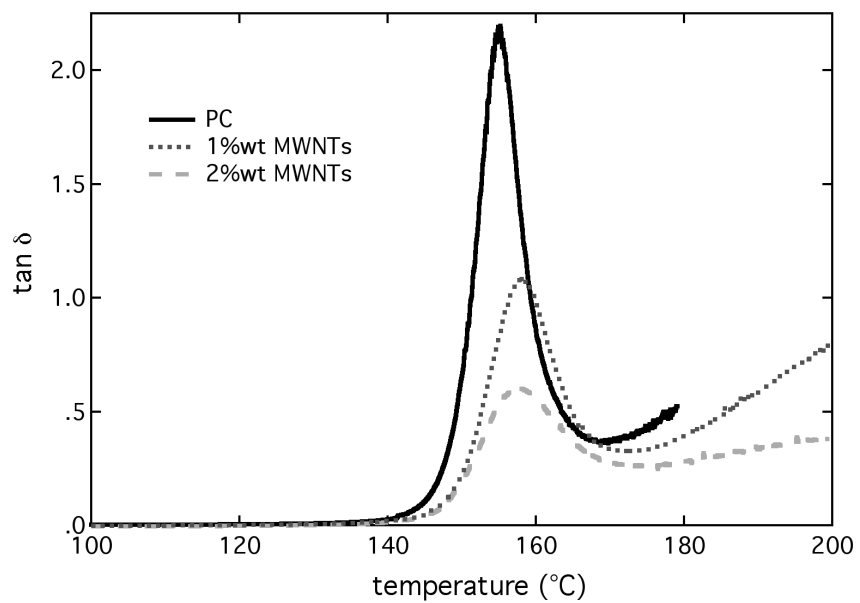
Figure 56. Loss tangent as a function of temperature for PC samples.

	E' at 60 °C (MPa)	E' at 180 °C (MPa)	T_g from E'' (°C)	T_g from tan δ (°C)[14]
PC	2090	2.9	150.0	155.2
1% MWNT	1954	9.2	152.6	158.3
2% MWNT	2640	47.6	152.3	157.3

Table 9. Comparison of storage moduli and glass transition temperatures for polycarbonate-based samples.

In Figure 54 we see an increase in the storage modulus for the 2 wt% MWNT sample, when compared to the response of the pure polycarbonate sample, at both low and high temperatures. While a similar improvement is not seen with the 1 wt% MWNT sample at low temperatures, we see that the high temperature (above T_g) storage modulus of the sample is also greatly enhanced. (Because of the large modulus increase at higher temperatures, we believe that this slight decrease in storage modulus at low temperatures is due to experimental error.) Storage moduli values for each sample at temperatures of 60 °C and 180 °C are compared in Table 9. As discussed earlier, this drastic improvement in high temperature properties has also been identified in the literature.

Both the loss moduli (Figure 55) and loss tangent (Figure 56) curves show slight shifting of the peak location upon the addition of nanotubes. (It is unclear at this

---

[14] The peak of the loss tangent curve is typically a few degrees greater than the location of the peak in the loss moduli data.

time why the shift for 1 wt% MWNT is slightly larger than that for the 2 wt% sample, and replicate sample testing has not been possible in order to verify this result. This anomaly will be investigated in future experiments.) Also evident is a slight broadening of the peaks of these curves, which is most apparent in the loss tangent data in Figure 56 (which is plotted over a smaller temperature range from 100 to 200°C). As discussed previously, we believe that this broadening is indicative of an increase in the range of molecular mobility within the system. Because this broadening seems to predominantly occur on the high temperature side of the peaks, this suggests that the NTs are reducing the molecular mobility of certain polymer regions within the NRP. This is consistent with our hypothesis of a reduced mobility interphase region surrounding the nanotube. In Figure 56, we also see a decrease in the magnitude of the peaks of the loss tangent curves, which is due to the reduced fraction of bulk polymer within the material. Note that the maximum value of the loss tangent decreases by a factor of 2 with the addition of 1 wt% MWNTs, and then decreases by another factor of 2 for the 2 wt% sample.

While the slight shift in T_g and the broadening of the loss modulus peaks (on the high temperature side) are qualitatively sensible based on our hypothesis of a reduced mobility polymer phase surrounding the nanotubes, quantitative predictive models of how the mobility of the polymer chains influences the glass transition temperature do not exist. Thus we were led to investigate the relaxation spectra of the

NRP and the physical aging characteristics of the material. The results from these areas of investigations are presented below.

Frequency- and Time-Domain Response of Nanotube-reinforced Polycarbonate

Dynamic mechanical analysis was also used to study the frequency-domain response of the polycarbonate-samples. Such tests provide another means with which to analyze the impact of the embedded nanotubes on the effective viscoelastic properties of the NRP. Frequency domain analysis lends itself quite nicely to micromechanical modeling of the effective response, which is accomplished by using appropriate elasticity solutions transformed into the frequency domain via the Dynamic Correspondence Principle. The specifics of the data collection techniques used to obtain the frequency domain data were discussed earlier in this chapter.

After describing the analysis of the frequency domain data and discussing the various responses (frequency domain, time domain, and relaxation spectrum) that we have obtained for the samples, we will demonstrate a frequency-domain micromechanical modeling approach using the Mori-Tanaka solution for a three dimensional random orientation of inclusions. By modeling the viscoelastic behavior of the interphase region as simply a change in the relaxation times of the bulk

polycarbonate response, via the mobility parameter α, it is possible to infer the behavior of this non-bulk polymer phase from experimental data obtained via macroscale mechanical testing of the bulk and reinforced polycarbonate samples. Such a model will be useful in interpreting experimental stiffness data obtained for nanotube-reinforced polymers and assessing changes in the mobility and mechanical behavior of the interphase region.

Analysis of frequency-domain data

Initial complex moduli data were collected over a range of frequencies (limited by the 0.01 to 200 Hz frequency range of the DMA machine) for temperatures ranging from approximately $T_g - 50$ °C to $T_g + 50$ °C. Then using the principle of time-temperature superposition, the moduli at different temperatures were shifted to form a reference curve at 150°C. Time-temperature superposition was carried out using software provided by the DMA manufacturer (TA Instruments, Thermal Analysis®), and a single temperature shift factor a_T chosen to provide the best fit for *both* storage and loss moduli data at a given temperature. An example of the raw data collected for a pure polycarbonate sample and shifted appropriately is shown in Figure 57. The nature of the anomalous behavior of the loss moduli curves at high frequencies is unknown but has been seen in the literature (Ferry 1980). Interestingly, most references to frequency-domain time-temperature superposition only consider the

storage modulus, and thus the behavior evident here is not typically discussed in the literature. In order to eliminate this behavior from our subsequent analysis, we will limit the upper frequency in our analysis to 10^5 Hz. Further investigation of this phenomena is warranted.

At this step in the analysis the storage and loss moduli data were fit to a 30-term Prony series using a linear least squares solver DYNAMFIT developed at Northwestern (Bradshaw and Brinson 1997b). The program assumes that the relaxation times τ_j are equally spaced in log time, and then calculates the Prony coefficients E_∞ and E_j which best fit the data, equally weighing storage and loss moduli contributions to the root mean square error (rms) of the solution. An extra constraint imposed within the code forces all Prony coefficients E_j to be greater than zero; while such a constraint does slightly increase the rms error describing the fit, negative Prony coefficients are not physically reasonable and thus were not considered. Typical rms values for the Prony series curve fit were under 10%, and usually within 0.2% of the rms value for the Prony series fit which did not include the positive coefficient constraint.
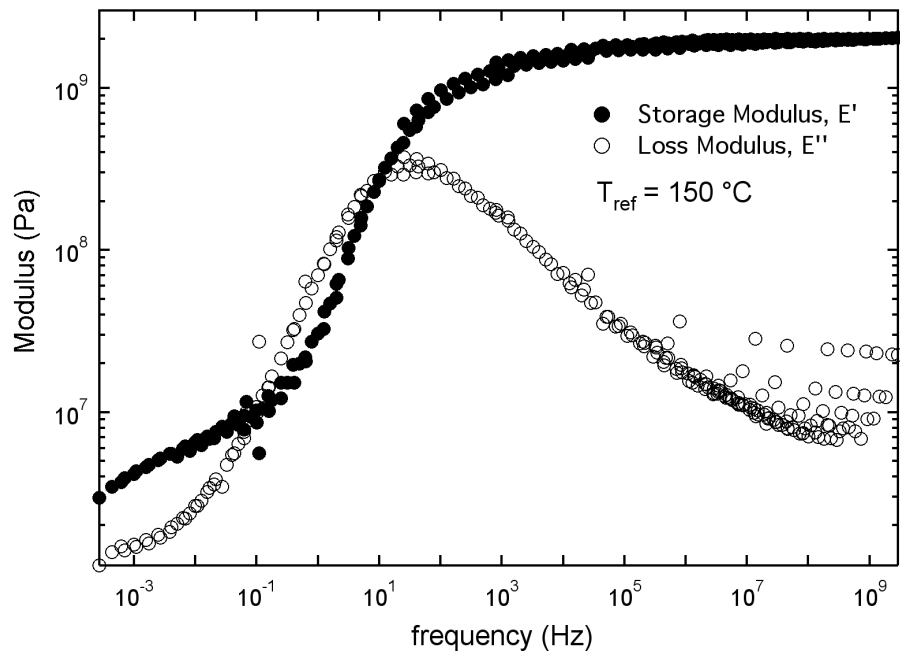
Figure 57. Time-temperature shifted frequency-domain experimental data for a pure polycarbonate sample.

An example of the Prony series fit to the experimental data for the case of pure polycarbonate (to a maximum frequency of 10^5) is shown in Figure 58. Once the Prony series terms have been obtained from the frequency-domain experimental data, the corresponding time-domain response and relaxation spectrum can be readily determined. The viscoelastic behavior for the blank and reinforced polycarbonate samples was characterized using this procedure and is described below.
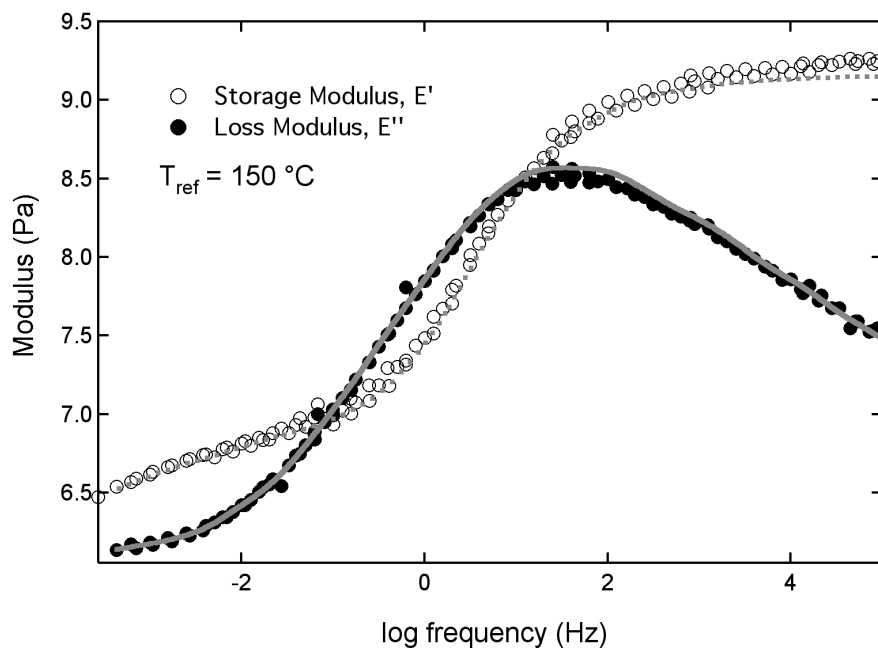
Figure 58. Prony series representation of the frequency domain data.

Experimental time and frequency domain response

Using the procedure outlined above, the shifted storage and loss moduli of the polycarbonate samples as a function of frequency for a reference temperature of 150°C are shown in Figure 59 and Figure 60, respectively. The corresponding time response of the samples, predicted based on the Prony series coefficients found from analysis of frequency domain data, is shown in Figure 61. Similar to the results obtained in the temperature scan experiments, we see a large increase in the low frequency storage modulus (and a corresponding increase in E(t) at long times) with the use of the carbon nanotubes as a filler phase. The peaks of the loss modulus curves

are slightly shifted to higher frequencies as the percentage of nanotubes is increased,

which is characteristic of a reduction in the effective molecular mobility of the sample.
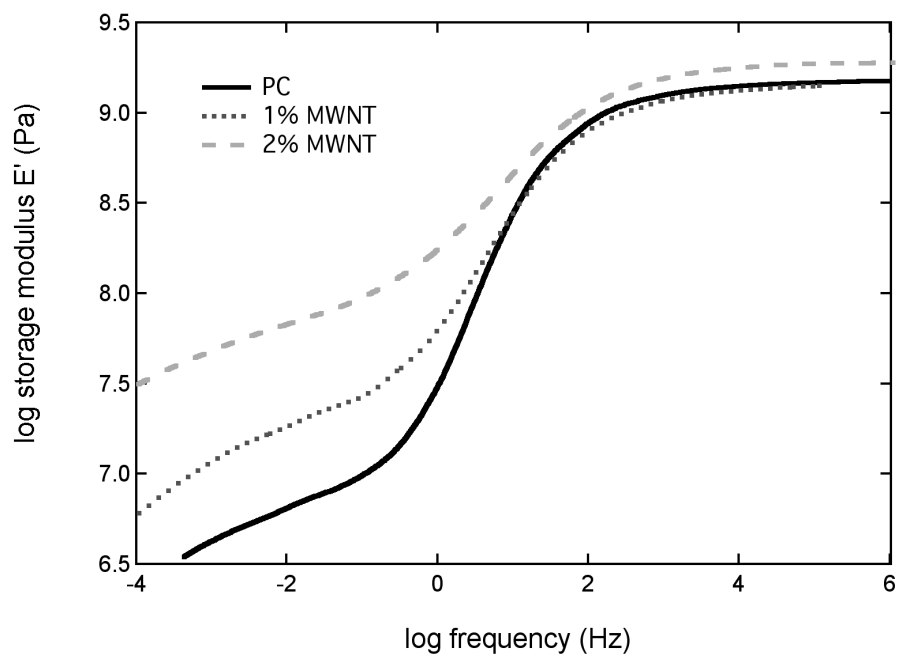
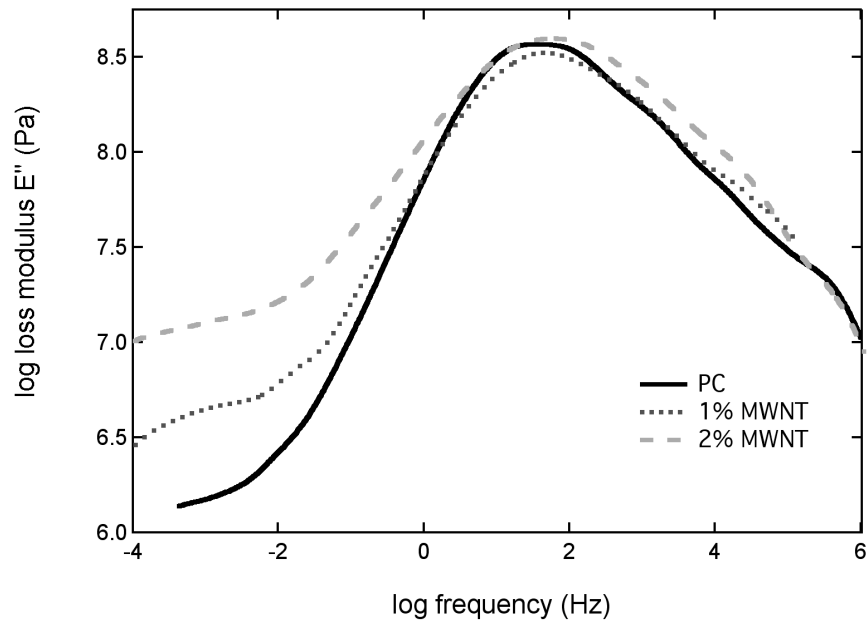**Figure 59. Frequency domain storage modulus for PC samples. T_{ref} = 150°C.**

Figure 60. Frequency domain loss modulus for PC samples. T_{ref} = 150°C.
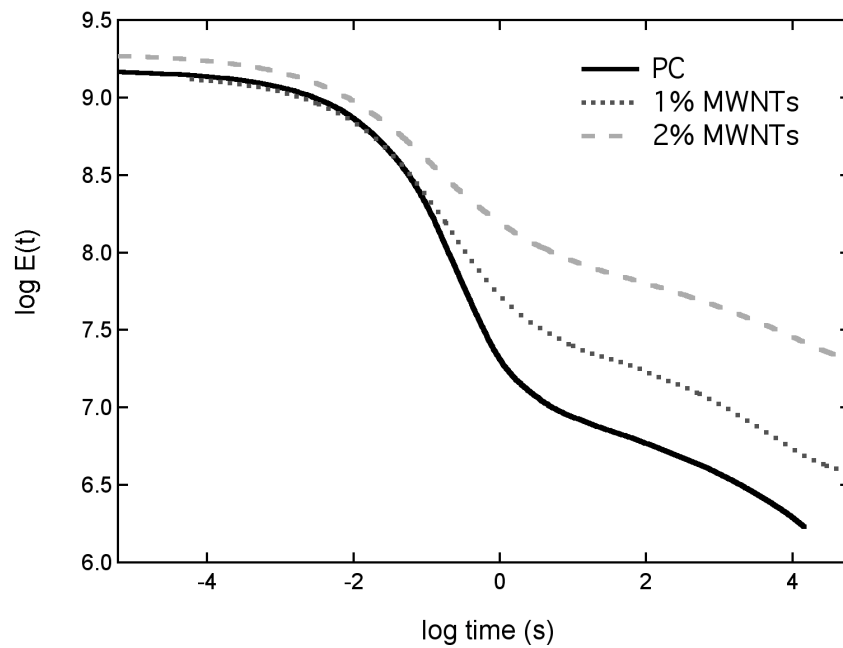
Figure 61. Time domain response for PC samples. T_{ref} = 150°C.

The relaxation spectra for the blank and reinforced polycarbonate samples are shown in Figure 62. Here we see an increase in the relaxation spectrum at longer times with increasing nanotube volume fraction. Also apparent is a slight broadening of the primary relaxation peak towards longer times. The broadening of the primary relaxation peak and the increase in the relaxation spectrum at longer times are both indicative of an increased number of relaxation modes and the introduction of longer time relaxation processes within the reinforced samples. These changes are consistent with the hypothesis of a reduction in molecular mobility within the interphase. Meanwhile, the location of the primary relaxation peak does not appreciably change with the addition of the nanotubes, suggesting that the primary relaxation mechanism within the NRP is the same as that within the bulk polymer sample. This is yet more evidence that the nanotubes *only* reduce the molecular mobility of the interphase region, and that polymer chains well separated from the nanotubes are not affected by the presence of the nanotubes and retain the mobility of the bulk polymer sample. These results are consistent with the three phase (NT-interphase-polymer) model presented in Figure 42.
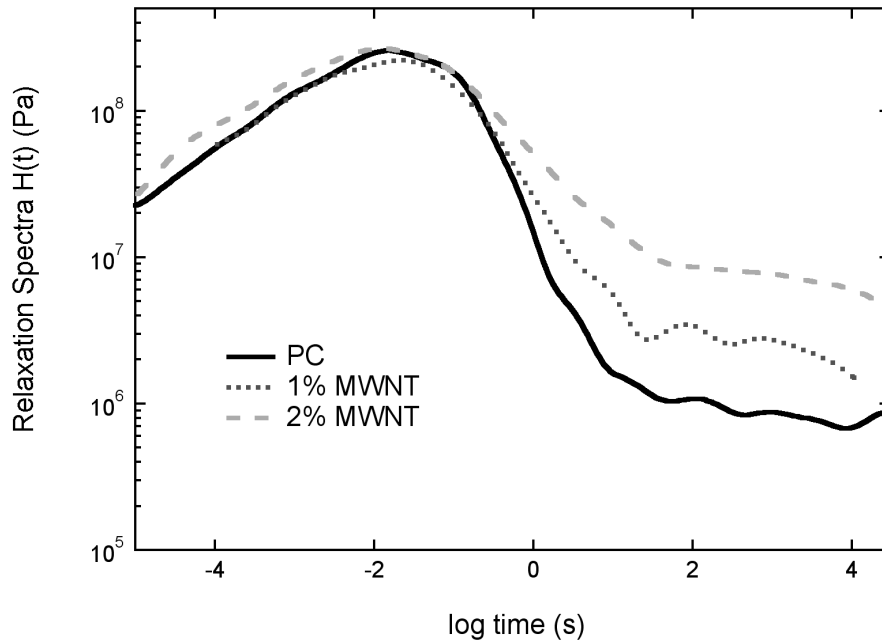
Figure 62. Relaxation spectra for PC samples. T_{ref} = 150°C.

Micromechanical modeling of NRP frequency domain behavior

One of the advantages of analyzing the frequency domain response of nanotube-reinforced polymers is that micromechanical models are available for the analysis and interpretation of results. This is accomplished by use of the Dynamic Correspondence Principle, which allows suitable elasticity solutions to be extended for the study of viscoelastic materials. One can show that there is a direct analogy between elasticity problems in the time domain and viscoelasticity problems in the frequency domain when the elastic moduli are replaced by their corresponding complex viscoelastic moduli of the form $\overline{E}^* = E' + iE''$, and associated field quantities

are allowed to be complex (Hashin 1965; Hashin 1970; Fisher 1998). Thus the Mori-Tanaka solution for a multiphase composite with viscoelastic phase materials can be written as (see Chapter 3)

$$\overline{L}^* = \left(\sum_{r=1}^{N} c_r \left\{ \overline{L}_r^* \, \overline{A}_r^* \right\} + c_0 \, \overline{L}_0^* \right) \left(\sum_{r=0}^{N} c_r \left\{ \overline{A}_r^* \right\} \right)^{-1} \tag{73}$$

The dynamic correspondence principle has been used by a variety of researchers to model the viscoelastic behavior of materials, and in particular has been used in conjunction with the Mori-Tanaka method to look at the effective viscoelastic moduli of a three phase composite with viscoelastic interphase and matrix phases (Fisher 1998; Fisher and Brinson 2001). As shown in Figure 63, the viscoelastic Mori-Tanaka model closely follows the results of a corresponding viscoelastic finite element model for the effective storage and loss transverse modulus of a 60% fiber-10% interphase-30% matrix unidirectional composite (Fisher and Brinson 2001). Particularly encouraging is the relative agreement between the two solutions within the transition region. Based on this result we feel that the use of a viscoelastic implementation of the Mori-Tanaka method is warranted.[15]

---

[15] Note that in Figure 63 the viscoelastic behavior of the interphase and matrix material were described by two distinct sets of Prony series coefficients (Fisher 1998).
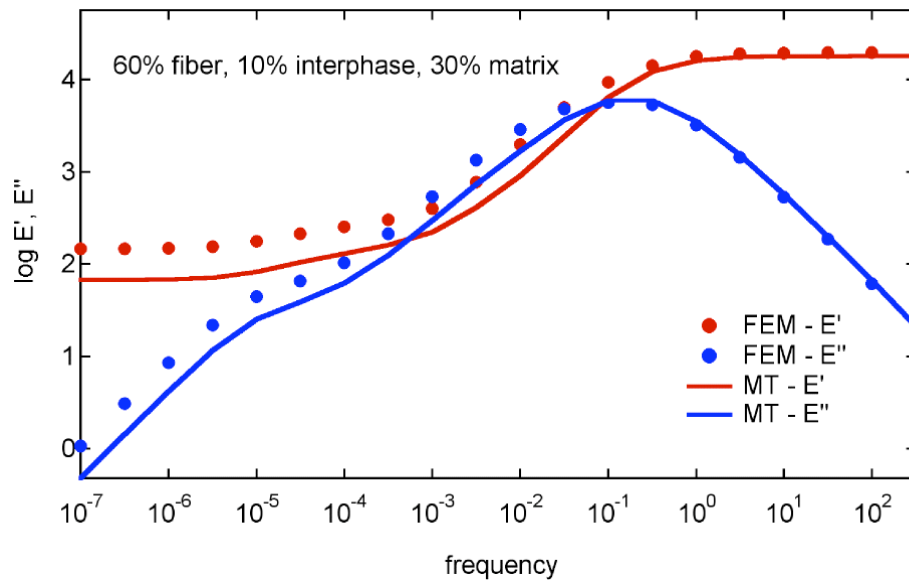
Figure 63. Comparison of Mori-Tanaka and finite element solutions for the transverse modulus of a three phase unidirectional composite with viscoelastic interphase and matrix phases. (Fisher 1998)

Initial micromechanical modeling results for the effective frequency domain response for the 2 wt% nanotube-reinforced polycarbonate samples are shown in Figure 64 and Figure 65. For the NRP composite, the viscoelastic matrix properties were assumed equal to those obtained for the bulk polycarbonate samples tested, and a 3D random orientation of NTs was assumed. The interphase volume fraction was chosen through a process of trial and error as 10%, and the interphase viscoelastic response was modeled as a simple shift in relaxation times of the pure polymer using the mobility parameter $\alpha=1000$ (also found through trial and error). For each of the NRP samples, the volume fraction of the nanotubes was assumed to be known (based

on the weight fraction of embedded nanotubes), and a nanotube (elastic) modulus of 200 GPa was chosen by fitting the high frequency portion of the Mori-Tanaka effective storage modulus to the experimental storage modulus of the NRP (see Figure 65).[16]
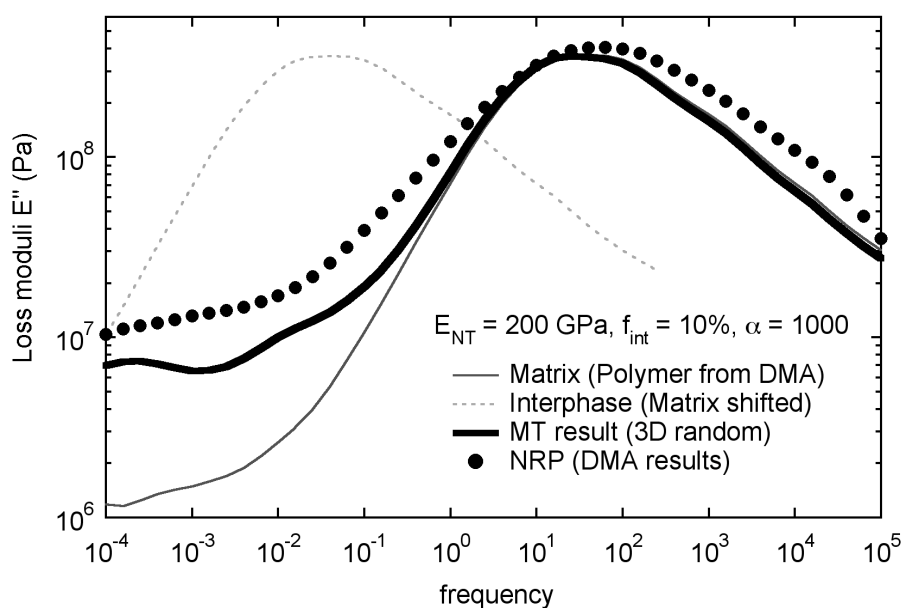

Figure 64. Mori-Tanaka prediction for 2% MWNT sample loss modulus, assuming f_{int}=10% and α=1000.

---

[16] A general rule of thumb for the conversion of weight fraction to volume fraction of nanotubes is to divide by a factor of two. This approximation was used here as the exact relationship between the densities of the nanotubes and the polymer was not known.
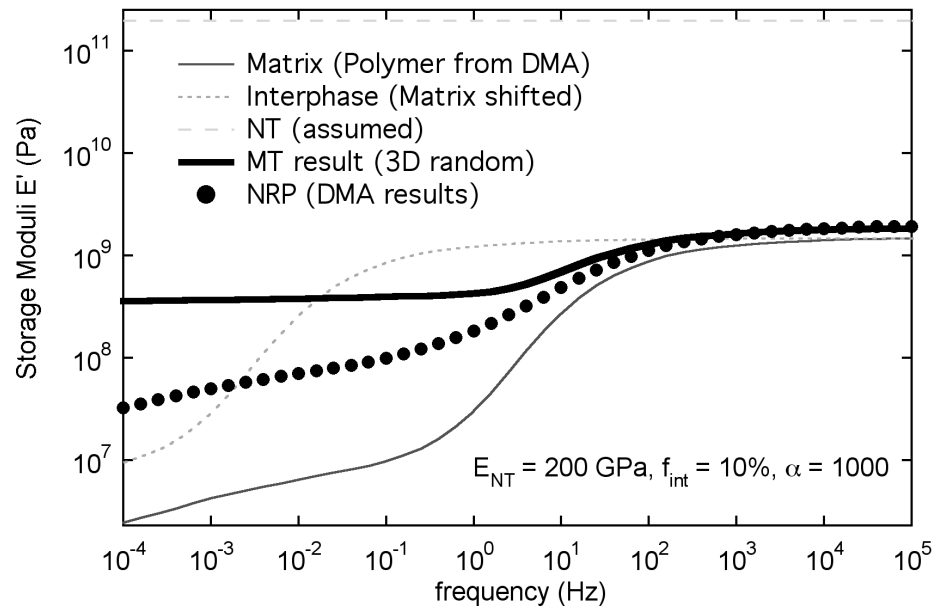
Figure 65. Mori-Tanaka prediction for 2% MWNT sample storage modulus, assuming f_{int}=10% and α=1000.

We are most interested in comparing the micromechanical solution with the experimental data for the loss modulus of the material, as the mechanical properties of the (elastic) nanotube should not factor in this analysis. In Figure 64, a comparison of the Mori-Tanaka prediction with the experimental NRP data for the effective loss modulus shows that qualitative agreement between the two is obtained when using an interphase volume fraction of 10% and a mobility parameter α=1000. We are particularly interested in the low frequency response of the loss modulus, where the micromechanical predictions increase from that of the pure polymer and approach the NRP experimental data as the α increases. (For comparison, Figure 66 shows the

Mori-Tanaka prediction for α=100.) Referring to Figure 65, we see that the Mori-Tanaka solution over-predicts (by an order of magnitude) the low frequency effective NRP *storage* modulus that was measured experimentally. This is directly related to the difficulties in predicting the elastic properties of NRPs using micromechanical methods. As discussed in Chapter 3, these over-predictions could be due to a number of factors, including poor NT-polymer interfacial behavior, inadequate NT dispersion, and embedded nanotube waviness.
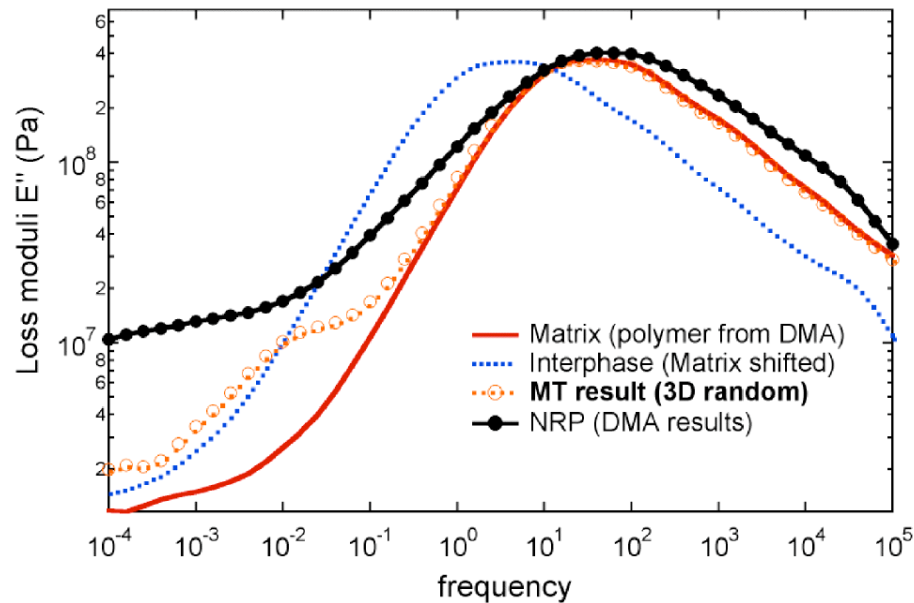

Figure 66. Mori-Tanaka prediction for 2% MWNT sample loss modulus, assuming f$_{int}$=10% and α=100.

Figure 67 compares the Mori-Tanaka prediction and the experimental data for the effective loss modulus for the 1% MWNT-PC sample. Using the same values for the interphase volume fraction (10%) and the mobility parameter α (=1000), we again see very good qualitative agreement between the Mori-Tanaka model and the experimental data.

These initial modeling efforts are illustrative of the future research directions for this work. As more data is collected, we will seek to fit the volume fraction and viscoelastic behavior of the interphase to experimental data collected over a range of nanotube volume fractions using the procedure demonstrated briefly above. However, the initial work presented here demonstrates that the impact of the nanotubes on the effective viscoelastic behavior of the NRP can be modeled using a three-phase Mori-Tanaka model. Furthermore, given the simple model of the interphase viscoelastic properties used here, we see that a relatively large volume fraction of interphase (10%) with significantly reduced mobility (three orders of magnitude) provides qualitative agreement between our micromechanical model predictions and the experimentally obtained data. Eventually, we foresee basing models of the interphase viscoelastic properties on nanoscale experimental data and/or molecular dynamics simulations of the NT-polymer system.
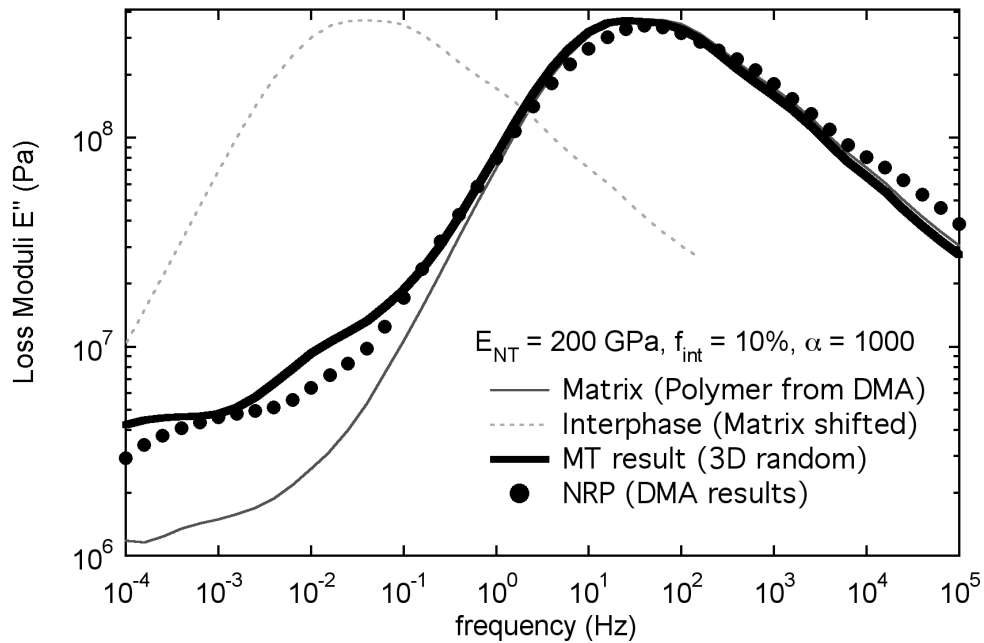
Figure 67. Mori-Tanaka prediction for 1% MWNT sample loss modulus, assuming f_{int}=10% and α=1000.

Physical Aging of Nanotube-reinforced Polycarbonate

Physical aging tests were conducted on both blank and nanotube-reinforced polycarbonate samples to ascertain the effect of the nanotubes on the effective physical aging characteristics of the material. The experimental procedure used to conduct the physical aging tests was described earlier in this chapter. An isothermal aging/test temperature of 135 °C was used for all tests, which is sufficiently close to the nominal T_g of the polycarbonate, such that significant aging affects will take place over relatively short periods of time.

Two sets of rejuvenation parameters (T_{rej}, t_{rej}) were used in this work: 160 °C for 10 minutes and 165 °C for 15 minutes. The higher temperature / longer time rejuvenation procedure was used after initial tests on samples rejuvenated at the lower T_{rej} showed evidence that full rejuvenation (i.e. a full erasure of previous thermal history) was not achieved under these conditions. We believe this to be the case because shift rates much smaller than one were obtained based on an analysis of the experimental data. In all cases, shift rates decreased as the weight fraction of the nanotubes increased.

Momentary creep compliance curves, and their shifting to form a master reference curve at the longest aging time, for a blank polycarbonate sample rejuvenated at 165 °C for 15 minutes were shown in Figure 46 and Figure 47, respectively. Corresponding plots for the 2% MWNT-PC samples tested using the same rejuvenation procedure are shown in Figure 68 and Figure 69. As expected, the compliance values of the 2% MWNT-PC sample are smaller then those for the blank PC, indicating a stiffer (higher modulus) response for the reinforced samples.
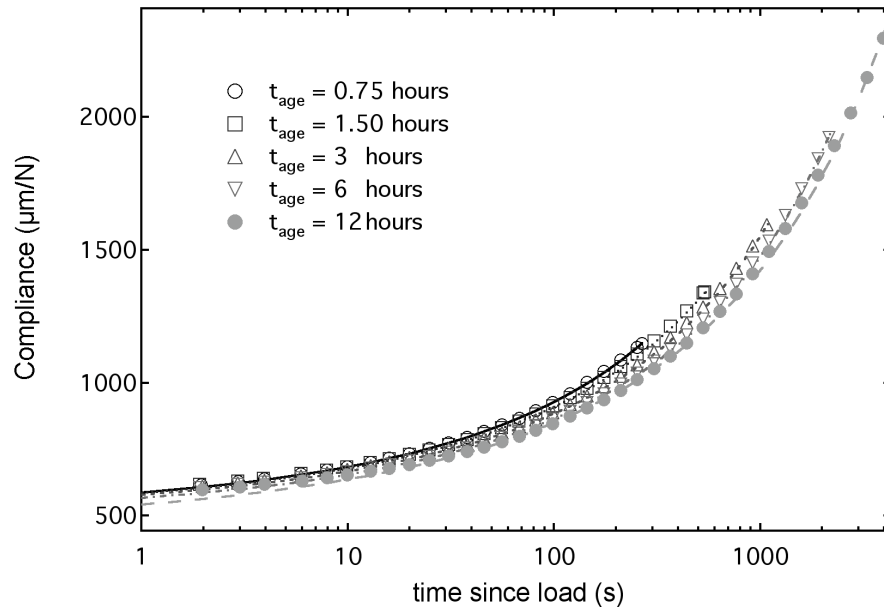
**Figure 68. Momentary compliance curves for 2% MWNT-PC sample
rejuvenated at 165 °C for 15 minutes.**

A qualitative comparison of the momentary creep compliance curves suggests that while the shapes of the curves are quite similar, the amount of shifting necessary to superpose the curves at the longest aging time (aging time shift factor a_{t_e}) is quite different. The shift factors for the blank and NT-reinforced samples are plotted as a function of aging time in Figure 70 and Figure 71 for the each of the two rejuvenation methods (160 °C for 10 minutes and 165 °C for 15 minutes), respectively. The shift rates calculated from this data are given in Table 10.
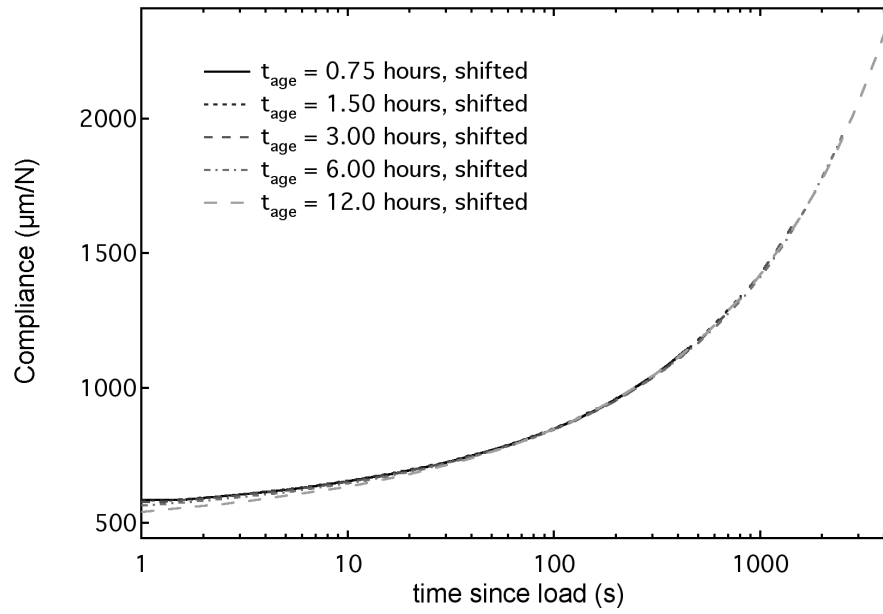
Figure 69. Shifting of momentary compliance curves for 2% MWNT-PC sample rejuvenated at 165 °C for 15 minutes.
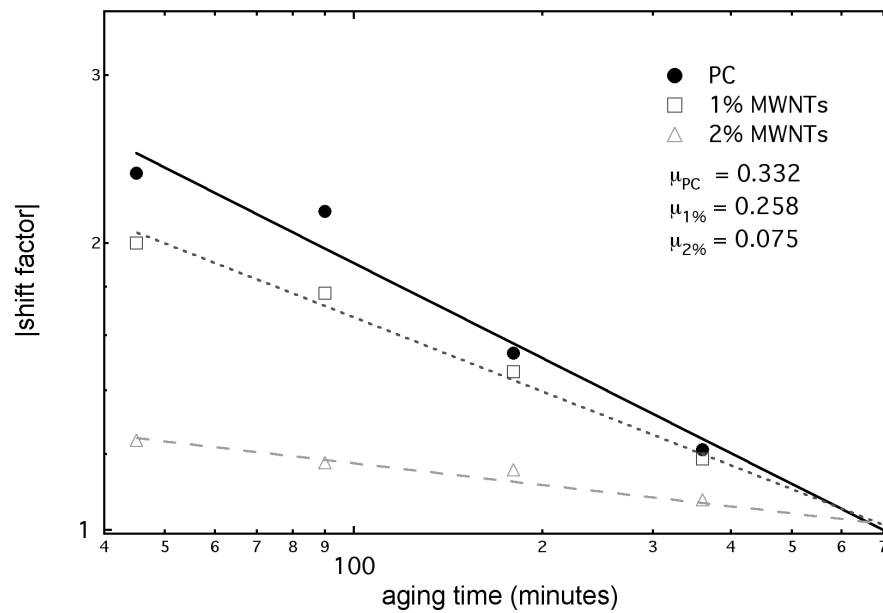

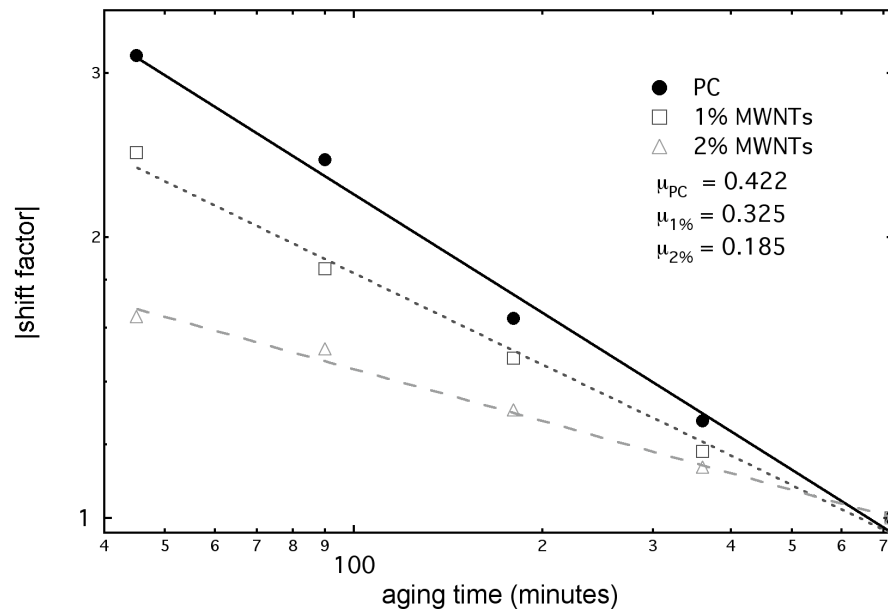**Figure 70. Shift rate μ for 160 °C rejuvenation for 10 minutes.**

Figure 71. Shift rate μ for 165 °C rejuvenation for 15 minutes.

Rejuvenation procedure	RPI PC sample	Shift rate (data)	Shift rate (PHYAGE)
160 °C for 10 minutes	Blank	0.332	0.325
	1% MWNTs	0.258	0.260
	2% MWNTs	0.075	0.082
165 °C for 15 minutes	Blank	0.422	0.405
	1% MWNTs	0.325	0.307
	2% MWNTs	0.185	0.187

Table 10. Shift rates of blank and NT-reinforced polycarbonate samples.

The shift rates determined for each of the samples are consistent with the hypothesis that the effective mobility of the nanotube-reinforced samples is more restricted than that measured for the pure polycarbonate.[17] As the weight fraction of nanotubes (and thus the volume of the interphase region) increases, the effective shift rates of the material (for a given rejuvenation procedure) decrease. From the standpoint of free volume, this can be viewed as the NRP samples requiring longer periods of time for the molecular rearrangements that lead to physical aging to occur. The fact that the shift rates obtained for the higher temperature / longer time rejuvenation are greater than those obtained for the lower temperature rejuvenation suggests that the former erased "more" of the prior thermal history of the sample. However, because these experimental shift rates are still much lower than unity, we believe that full rejuvenation of the samples (particularly the nanotube-reinforced samples) may not have been achieved. Optimal rejuvenation parameters for these samples will be the subject of future work. Nonetheless, the following conclusions can be drawn based on the physical aging tests conducted to date:

---

[17] At this moment it is impossible to rule out the possibility that the differences in rejuvenation is solely caused by the change in effective T_g of the material due to the presence of the nanotubes. Once a full rejuvenation protocol has been established, we will be able to analyze this possibility in greater detail. Nonetheless, we anticipate that the embedded nanotubes will result in different physical aging behavior between the blank and NT-reinforced samples.

∞   The embedded nanotubes significantly influence the rejuvenation of the polycarbonate samples,

∞   Shift rates for (partially) rejuvenated samples decrease as the weight fraction of nanotubes increase; we attribute this to an interphase region surrounding the nanotubes,

∞   The shift rate behavior can be described qualitatively using the concept of a reduced mobility, non-bulk polymer interphase region,

∞   This reduced mobility interphase region is consistent with the results of other viscoelastic testing (T_g and relaxation spectra) that have been measured for these same polycarbonate-based samples, and

∞   These results suggest that changes in the physical aging behavior of the NRP may be sensitive to changes in molecular mobility, such that physical aging studies may be useful in evaluating such changes in nanotube-reinforced polymer systems.

Currently we are in the process of re-evaluating the rejuvenation procedure in order to develop a protocol which completely erases the thermal history of the samples, without compromising the structure or properties of the samples. Once this has been completed, physical aging tests will be re-run on each of the samples described in this work, as well as additional samples with other weight fractions of

nanotubes which we hope to receive shortly. Based on the preliminary physical aging results presented here, we feel that the nanotubes will significantly alter the aging characteristics of the NRP (with respect to the pure polymer), and as such appreciably impact the long-term viscoelastic behavior of the NRP.

Summary

We have compared the effective viscoelastic response of pure and nanotube-reinforced polycarbonate samples using dynamic mechanical analysis. Three types of viscoelastic behavior were analyzed: the glass transition temperature, the frequency response, and physical aging. The results of each of these tests demonstrate that the effective viscoelastic behavior of the nanotube-reinforced polymer is consistent with the hypothesis that a reduced mobility, non-bulk polymer interphase forms in the region surrounding the nanotube. This reduction in mobility is believed to be due to the nanostructure of the NRP, and is attributed to interactions between the polymer chains and the nanotubes.

Preliminary micromechanical modeling suggests that this interphase region may be quite large (several times the volume fraction of the nanotubes) and have viscoelastic properties quite different from those of the bulk polymer (a three order of magnitude shift in relaxation times using the simple model described here). While

such modeling may assist in the interpretation of experimental data, the utility of the predictions are limited due to the number of assumptions that are implicit within the model. In the next chapter we will discuss proposed future experiments on a novel nanotube-reinforced polymer system, based on an ordered and uniform carbon nanotube array. The promise of such a system is that the large degree of control with respect to the composite geometry greatly simplifies the mechanical modeling of the effective response.